# Optical Excitation of Propagating Magnetostatic Waves in an Epitaxial Galfenol Film by Ultrafast Magnetic Anisotropy Change

N.E. Khokhlov,[1,*] P.I. Gerevenkov,[1] L.A. Shelukhin,[1] A.V. Azovtsev,[1] N.A. Pertsev,[1] M. Wang,[2] A.W. Rushforth,[2] A.V. Scherbakov,[1,3] and A.M. Kalashnikova[1]

[1] *Ioffe Institute, 194021 St. Petersburg, Russia*

[2] *School of Physics and Astronomy, The University of Nottingham, NG7 2RD Nottingham, United Kingdom*

[3] *Experimental Physics II, Technical University Dortmund, D44227 Dortmund, Germany*

(Received 11 April 2019; revised manuscript received 24 July 2019; published 18 October 2019)

Using a time-resolved optically pumped scanning-optical-microscopy technique, we demonstrate the laser-driven excitation and propagation of spin waves in a 20-nm film of a ferromagnetic metallic alloy Galfenol epitaxially grown on a GaAs substrate. In contrast to previous all-optical studies of spin waves, we employ laser-induced thermal changes of magnetocrystalline anisotropy as an excitation mechanism. A tightly focused 70-fs laser pulse excites packets of magnetostatic surface waves with an $e^{-1}$-propagation length of 3.4 $\mu$m, which is comparable with that of permalloy. As a result, laser-driven magnetostatic spin waves are clearly detectable at distances in excess of 10 $\mu$m, which promotes epitaxial Galfenol films to the limited family of materials suitable for magnonic devices. A pronounced in-plane magnetocrystalline anisotropy of the Galfenol film offers an additional degree of freedom for manipulating the spin waves' parameters. Reorientation of an in-plane external magnetic field relative to the crystallographic axes of the sample tunes the frequency, amplitude, and propagation length of the excited waves.

DOI: 10.1103/PhysRevApplied.12.044044

## I. INTRODUCTION

In magnonics, coherent spin waves (SWs) are employed for encoding, transferring, and processing information [1–3]. The use of SWs enables scaling of magnonic elements down to the nanometer range owing to short wavelengths and the reduction of Joule heating associated with the charge transfer in conventional electronics. Moreover, an extended functionality of magnonic devices is provided by the possibility to manipulate the amplitudes, phases, and wave vectors of SWs. Progress in the field of magnonics relies on the development of approaches to generate and transfer SWs in a controllable manner. Efficient conversion mechanisms between electrical or optical pulses and collective magnetic excitations are required to couple magnonic elements to electronic and photonic units [4–6]. For rapid growth of the field of magnonics, it is essential to extend the range of materials and structures supporting long-propagation-distance SWs and enabling their control [7–11].

Optical radiation allows the magnetic parameters of materials to be altered reversibly at various timescales down to femtoseconds [12,13]. This has led to the emergence of photomagnonics [14–20], where laser pulses are employed as a tool for both driving SWs and manipulating their propagation. In particular, it has been demonstrated that femtosecond laser pulses enable excitation of SWs with controlled wave vectors and propagation directions [18,21–23]. However, up to now, the effects of short laser pulses employed to drive SWs have been limited to ultrafast optomagnetic phenomena [18,21,22,22–25], ultrafast demagnetization [17,26–29], and coherent energy transfer from elastic waves to the magnon subsystem [24,30–33]. These mechanisms place constraints on the properties of the media, the laser pulse parameters, and the excitation geometries, while the excitation of propagating SWs by other ultrafast magnetic phenomena [13] remains unexplored. Furthermore, the range of materials where the optical generation of SWs has been realized is also very limited and, in fact, coincides with the known suitable media for magnonics [3].

In this article, we examine the feasibility and advantages of excitation of propagating SWs in an anisotropic ferromagnetic film by ultrafast laser-induced thermal changes of the magnetocrystalline anisotropy. Using time-resolved optically pumped scanning optical microscopy (TROPSOM) [17], we reveal propagating magnetostatic surface waves (MSSWs) excited by a femtosecond laser pulse in a thin film of a ferromagnetic metallic alloy Galfenol $Fe_{0.81}Ga_{0.19}$ epitaxially grown on a

*n.e.khokhlov@mail.ioffe.ru

 

GaAs substrate. We demonstrate that the propagating MSSW packets are launched via the laser-induced thermal decrease of the magnetic anisotropy occurring on a picosecond timescale and localized within the excitation spot. Owing to this excitation mechanism, the MSSWs are excited in a simple geometry with an in-plane external magnetic field, and their characteristics can be controlled by the orientation of the in-plane field with respect to the magnetocrystalline anisotropy axes of the film. We show that the 20-nm-thick Galfenol film supports an $e^{-1}$-propagation length of MSSWs as large as 3.4 $\mu$m, comparable to that of permalloy — a model metallic material for magnonics [3]. Our results promote epitaxial Galfenol to the limited family of materials for magnon spintronics, reconfigurable magnonics, and ultrafast photomagnonics. Furthermore, the ultrafast thermal changes of magnetic anisotropy as a driving mechanism for the excitation of propagating SWs can be applied to a broad range of materials without specific constraints imposed on their electronic and magnetic structures [34].

The article is organized as follows. In Sec. II, we describe the $Fe_{0.81}Ga_{0.19}$/GaAs sample and the details of the TROPSOM experimental setup. In Sec. III, we first present the experimental results on laser-induced excitation of the magnetization precession and SWs (Sec. III A); discuss the excitation mechanism (Sec. III B) and the main parameters and features of the MSSW propagation (Sec. III C); and reconstruct the MSSW dispersion from experimental data (Sec. III D). This is followed by a theoretical analysis of the MSSW dispersion relation specific to the anisotropic $Fe_{0.81}Ga_{0.19}$ film, calculations of the main MSSW parameters, and their comparison to those obtained experimentally (Sec. III E). In Sec. IV, we summarize our findings and discuss their possible impact on the field of magnonics.

## II. EXPERIMENTAL DETAILS

### A. Sample

For our study, we choose a film of $Fe_{0.81}Ga_{0.19}$ with a thickness $d = 20$ nm epitaxially grown on a 350-$\mu$m-thick GaAs(001) substrate by magnetron sputtering, as described elsewhere [35]. The Galfenol film is capped with 3-nm-thick Al and 120-nm-thick $SiO_2$ protective layers. The back side of the substrate is polished to optical quality. X-ray diffractometry shows that the Galfenol film has a mosaic structure with grain sizes of approximately 12 nm and their crystallographic axes have a misorientation of approximately 1.3°. It is well established that thin films of iron and iron-based alloys epitaxially grown on GaAs exhibit intrinsic cubic and substrate-induced in-plane uniaxial magnetic anisotropies [36–39]. In particular, in Galfenol films on GaAs(001) substrates, the uniaxial anisotropy axis emerges along the [110] direction [35,40].

### B. Experimental setup

Optically excited SWs are studied using the TROPSOM setup, which enables detection of the spatial-temporal evolution of the polar magneto-optical Kerr rotation $\Delta\theta_K$ proportional to the transient changes of the out-of-plane magnetization component $M_z$ (Fig. 1). Here, $xyz$ is the laboratory frame with the $z$ axis directed along the sample normal and the $x$ axis is chosen to be along the direction of an external dc magnetic field **H**. Optical pulses with nominal duration of 70 fs, central wavelength of 1050 nm, and 70 MHz repetition rate generated by the Yb-doped solid-state oscillator laser system are split into pump and probe parts. The central wavelength of the pump pulses is converted to 525 nm using a $\beta$-$BaB_2O_4$ crystal. The amplitude of the pump pulses is periodically modulated at a frequency of 84 kHz using a photoelastic modulator placed between two crossed Glan-Taylor prisms. Two microscope objectives are used to focus the pump and probe pulses onto the Galfenol film from the cap and the substrate sides, respectively. The pump and probe radii $\sigma$, i.e., the half-width of the beam's spatial profile at which the intensity drops by $\sqrt{e}$, are measured to be 0.8 $\mu$m using the knife-edge method. The pump fluence is 3.5 mJ/cm$^2$, and the probe fluence is approximately 20 times lower. The micro-objective for the probe pulses is fixed. The micro-objective for the pump pulses is mounted on the piezoelectric stage, which moves in the $x$-$y$ plane and controls the relative spatial displacements $\Delta x, \Delta y$ between the pump and probe pulses. The pump-probe temporal delay $t$ is controlled by a delay line in the pump pulse optical path. In the experiments, the temporal dependences of the probe polarization

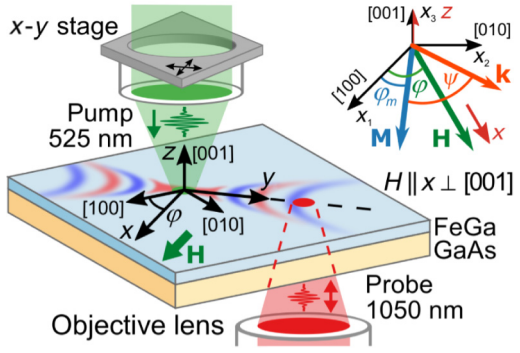


FIG. 1. Experimental geometry. A dc magnetic field **H** is applied along the $x$ axis, while the azimuthal orientation of the sample $\varphi$ can be varied. The relative pump-probe distance is changed along either the $x$ or $y$ direction to detect propagation of backward volume magnetostatic wave (BVMSW) or MSSW modes, respectively. The blue-red pattern represents SW propagation in the $x$-$y$ plane schematically. The inset shows the $x_1x_2x_3$ reference frame linked to the crystallographic axes of the sample, with the angles $\varphi_m$, $\varphi$, and $\psi$ defining the in-plane orientations of the magnetization **M**, external dc magnetic field **H**, and the SW wave vector **k**, respectively.

$\Delta\theta_K(t)$ are obtained at various pump-probe displacements $\Delta x$, $\Delta y$ and at various azimuthal orientations of the sample defined by the angle $\varphi$ between the [100] crystallographic axis and the $x$ axis. The probe polarization rotation $\Delta\theta_K(t)$ is detected using a conventional scheme with a Wollaston prism and a balanced photodetector. The signal from the photodetector is registered using a lock-in technique with the reference frequency of the pump amplitude modulation. Thus, only the probe polarization rotation related to the pump-induced dynamics is detected. The measurements of the propagating SWs are performed at room temperature and $H = 100$ mT.

## III. EXPERIMENTAL RESULTS AND DISCUSSION

### A. Laser-induced excitation of propagating spin waves

Figures 2(a) and 2(b) show the spatial-temporal evolution of $\Delta\theta_K$ obtained by scanning the pump-probe time delay $t$ when the pump and probe spots are shifted with respect to each other by $0 \le \Delta y \le 12$ $\mu$m at $\Delta x = 0$, i.e., transversely to **H**. Experimental data for two orientations of the sample $\varphi = 45°$ and $\varphi = 60°$ are presented. The former geometry corresponds to the field applied along the film's hard axis [110]. Two types of pump-induced signal $\Delta\theta_K(t)$ can be distinguished depending on whether the pump and probe spots overlap spatially or not. We show this in more detail in Fig. 2(c), where the cross sections of the spatial-temporal maps at various $\Delta y$ are presented. When the pump and probe spots overlap spatially, i.e., at $\Delta y < \sqrt{2}\sigma$, decaying oscillations of $\Delta\theta_K(t)$ are observed. Examination of the dependence of the oscillation frequency on the external field strength [Fig. 2(e)] confirms that they originate from the laser-induced precession of the magnetization. Outside the pump-probe spatial overlap, i.e., at $\Delta y > \sqrt{2}\sigma$, well-defined wavepackets are observed in the $\Delta\theta_K(t)$ signal. The tilts of the signal maxima reveal a positive phase shift of the propagating waves. Therefore, these wavepackets can be confidently ascribed to laser-induced MSSWs propagating transversely to **H**.

Spatial-temporal $\Delta x$-$t$ maps obtained at $\Delta y = 0$ [Fig. 2(d)] reveal the presence of fast-decaying BVMSWs with negative phase shifts. Such a difference in the propagation characters of laser-driven MSSWs and BVMSWs appears to be typical for thin metallic films [26–28]. Below, we focus our discussion on the excitation and propagation of the MSSWs.

As can be seen in Figs. 2(a) and 2(b), the parameters of the magnetization precession at $\Delta y = 0$ and of the MSSWs at $\Delta y \neq 0$ vary with $\varphi$. To quantify the azimuthal dependences of the parameters, we fit temporal signals $\Delta\theta_K(t)$ obtained at different $\varphi$ and $\Delta y$ with one

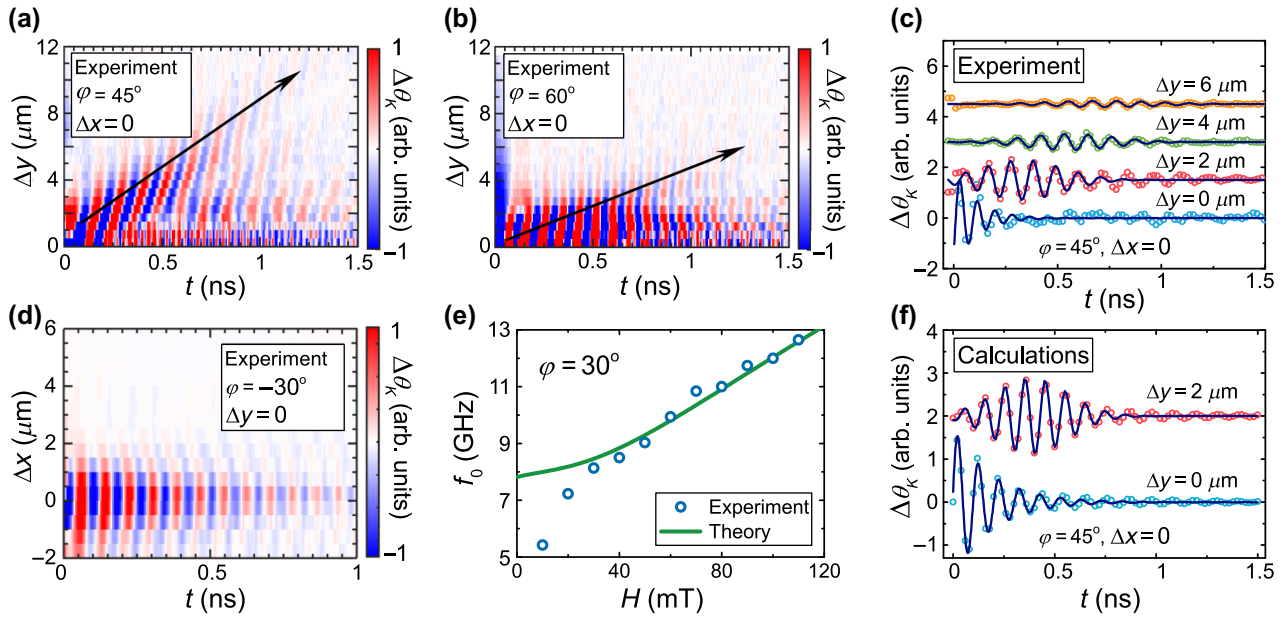


FIG. 2. (a),(b) Experimental spatial-temporal $\Delta y$-$t$ maps of $\Delta\theta_K$ obtained at $\varphi = 45°$ (a) and $\varphi = 60°$ (b) and $\Delta x = 0$, i.e., when the pump-probe distance $\Delta y$ is scanned transversely to **H**, corresponding to the MSSW configuration. Arrows are guides to the eye showing the centers of the propagating MSSW packets. (c) Experimental (symbols) temporal evolution of $\Delta\theta_K$ at different pump-probe distances $\Delta y$, at $\varphi = 45°$ and $\Delta x = 0$. Solid lines denote the fits using Eqs. (1) and (2). (d) Experimental spatial-temporal $\Delta x$-$t$ map of $\Delta\theta_K$ obtained at $\varphi = -30°$ and $\Delta y = 0$, i.e., when the pump-probe distance $\Delta x$ is scanned along **H**, corresponding to the BVMSW configuration. (e) Experimental (symbols) dependence of the precession frequency $f_0$ on the strength of the magnetic field $H$ applied at $\varphi = 30°$ and theoretical dependence (solid line) calculated using Eq. (5). (f) Calculated (symbols) temporal evolution of $\Delta\theta_K$ at different pump-probe distances $\Delta y$, at $\varphi = 45°$ and $\Delta x = 0$. Solid lines denote the fits using Eqs. (1) and (2).

of the functions:

$$\Delta\theta_K(\Delta y = 0, t) = A^0_{\rm SW}\sin(2\pi f_0 t - \phi_0)e^{-t/\tau}, \quad (1)$$

$$\Delta\theta_K(\Delta y, t) = A_{\rm SW}(\Delta y)\sin(2\pi f t - \phi)e^{-(t-t_0)^2/(2w^2)}. \quad (2)$$

Here, $A^0_{\rm SW}$ and $A_{\rm SW}(\Delta y)$ are amplitudes of the precession at $\Delta y = 0$ and $\Delta y > 0$, respectively; $\tau$, $f_0$ and $f$, and $\phi_0$ and $\phi$ are the decay time, frequencies, and initial phases of the precession, respectively; and $w$ and $t_0$ the width and center position of the Gaussian packet, respectively. Good agreement between the experimental data and the fitted curves is reached [Fig. 2(c)], apart from a small discrepancy at the tails of the precession and wavepackets, which is addressed below in Sec. III E.

### B. Mechanism of MSSW excitation

Figures 3(a) and 3(b) show the azimuthal dependences $f_0(\varphi)$ and $A^0_{\rm SW}(\varphi)$ at $\Delta y = 0$. The former has a pronounced fourfold symmetry with a twofold distortion. It corresponds well to the intrinsic cubic magnetic anisotropy defined by the anisotropy parameter $K_1 > 0$ with easy axes along [100] and [010] and the substrate-induced in-plane uniaxial magnetic anisotropy defined by the parameter $K_u < 0$ with an easy axis along [110] expected for such films [38].

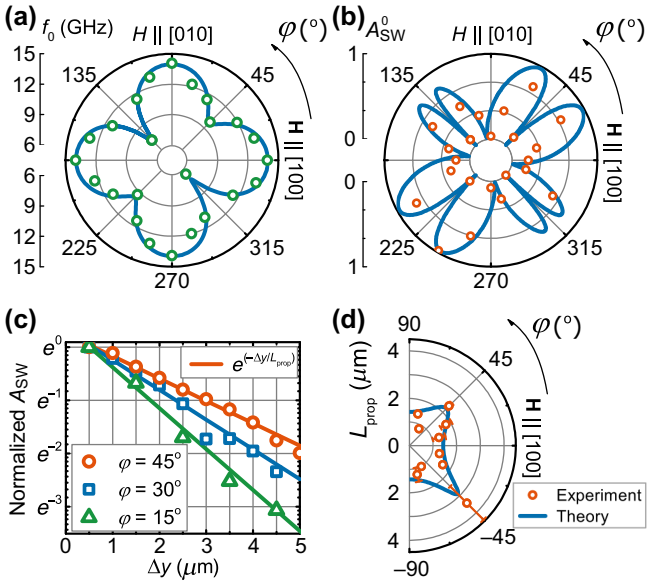


FIG. 3. (a),(b) Azimuthal dependences of the frequency $f_0$ (a) and amplitude $A^0_{\rm SW}$ (b) of the precession observed at $\Delta y = \Delta x = 0$. Symbols show experimental data; solid lines are the theoretical fits. (c) Normalized amplitude of MSSW packets $A_{\rm SW}(\Delta y)/A_{\rm SW}(\Delta y = 0.5\ \mu{\rm m})$ vs distance $\Delta y$ as obtained for several angles $\varphi$; lines are the fits using Eq. (3). (d) Propagation length $L_{\rm prop}$ of MSSW packets vs $\varphi$ as obtained from the experimental fits (symbols) and using Eq. (10) (solid line).

A pronounced azimuthal dependence of the amplitude $A^0_{\rm SW}(\varphi)$ of the laser-driven precession [Fig. 3(b)] allows us to identify the excitation mechanism as an ultrafast laser-induced *thermal* change of the effective magnetocrystalline anisotropy field demonstrated earlier for a range of Galfenol films of various thicknesses [41,42]. In brief, excitation of the precession stems from a rapid decrease of the anisotropy parameters $K_1$ and $K_u$ [43–45] and of the saturation magnetization $M_s$ [46] in response to the laser-induced increase of electronic and lattice temperatures. For the in-plane orientation of external magnetic field considered here, the amplitude of the excited precession is a measure of the abrupt reorientation of the total effective field in the sample plane due to the laser-induced changes of $K_1/M_s$ and $K_u/M_s$. At the timescale longer than the electron-phonon thermalization time of approximately 2 ps, the thermodynamic approximation for the temperature dependence of anisotropy can be applied [47]. Thus, the decrease of the parameters $K_1$ and $K_u$ is expected to be stronger than that of the magnetization $M_s$, and, therefore, the laser excitation yields an abrupt decrease of the effective anisotropy field. Experimentally verified independence of the $\Delta\theta_k(t)$ signal on the pump pulse's polarization supports the thermal nature of the excitation mechanism.

In the following, we refer to the MSSW excitation mechanism based on a laser-induced thermal change of the effective magnetocrystalline anisotropy field governed by the factors $K_1/M_s$ and $K_u/M_s$ as the ultrafast laser-induced change of the magnetic anisotropy. This is to distinguish it from the excitation of the MSSWs via ultrafast changes of the shape anisotropy solely related to the demagnetization and demonstrated in Refs. [17,26–29,48]. The latter mechanism is deliberately excluded here by the chosen experimental geometry with an in-plane external magnetic field. We can also exclude two other mechanisms of laser-induced MSSW excitation reported earlier. The ultrafast inverse magneto-optical effects employed in Refs. [18,21,22,22–25] are proven to be efficient in dielectric media mostly (for a review, see, e.g., [49]) and are pump-polarization sensitive, which is not the case in our experiments. Driving SWs by optically excited elastic waves as shown in Refs. [24,30–33] can, in turn, work in any material with sufficiently strong magnetoelastic coupling at any laser-pulse polarization. Furthermore, the magnetoelastic properties of Galfenol favor such a mechanism. However, the excitation of SWs by elastic waves becomes efficient only near the crossing of their dispersion curves [50], which is not realized in the studied film in the range of the applied magnetic fields used in the experiments (see details in Sec. III D). Nevertheless, in the experiments, we detect two acoustic waves seen as two concentric ripples independently propagating slower than the SWs, in analogy with the observations reported in Ref. [17].

### C. MSSW propagation length

The azimuthal dependence of the MSSW amplitude $A_{SW}(\varphi)$ at $\Delta y = 0.5$ $\mu$m, i.e., close to the edge of the excitation spot, naturally resembles the one for $A^0_{SW}$. At $\Delta y > \sqrt{2}\sigma$, the situation changes drastically, as the amplitudes of the MSSW packets outside the excitation spot are defined not only by the efficiency of excitation in the specific field direction [Fig. 3(b)], but by the spatial decay as well. To single out the latter contribution, we plot the spatial dependence of the normalized amplitudes of the MSSW packets $A_{SW}(\Delta y)/A_{SW}(\Delta y = 0.5\ \mu\text{m})$ [Fig. 3(c)]. The spatial decay has minima at $\varphi = \pm 45°$, i.e. in the so-called "hard-hard" configuration, where the equilibrium magnetization and the MSSW wave vector are oriented along the two orthogonal hard axes. Thus, the MSSW packets propagate larger distances along the hard axes, despite small initial amplitudes defined by the excitation mechanism. In contrast, no propagating MSSW packets are observed if **H** is directed close to the easy axes ($\varphi = 0°, \pm 90°$) and the small amplitude precession is excited.

The experimental dependences $A_{SW}(\Delta y)$ can be well fitted by a single exponential decay function [Fig. 3(c)]:

$$A_{SW}(\Delta y) \sim e^{-\Delta y / L_{prop}}, \tag{3}$$

with $L_{prop}$ being the propagation length. This is an important parameter of SWs, which, in particular, determines whether Galfenol is a suitable material for magnonic applications. As can be seen in Fig. 3(d), $L_{prop}$ demonstrates a pronounced azimuthal dependence with two maxima corresponding to the geometries with **H** applied along the hard axes. The largest $L_{prop} = 3.4$ $\mu$m is observed when **H** is aligned along the hardest anisotropy axis [$1\bar{1}0$]. Importantly, this value is very close to the propagation length found for optically excited MSSWs in a 20-nm-thick permalloy film [26].

### D. Reconstruction of MSSW dispersion

The $\Delta y - t$ maps presented in Figs. 2(a) and 2(b) allow us to reconstruct the dispersion relation $f(k_y)$ for the excited MSSWs using a two-dimensional fast Fourier transform (2D FFT) of the data outside the pump spot [24,27,32]. Figure 4(a) shows the 2D FFT result for $\varphi = 45°$, at which the MSSWs possess large $L_{prop}$ (see Sec. III C). The 2D FFT gives an expected near-linear dispersion and shows that the wave numbers $k_y$ of the MSSWs detected in the experiment reach about 3.5 rad/$\mu$m. As discussed in Ref. [27], the wave numbers of the SWs detected in the optical pump-probe experiment are limited by both the pump and probe spot sizes, which yields $k_\sigma = 1/\sigma$ for the wave numbers at the $1/\sqrt{e}$ level (see the Appendix for details). Given the spot size $\sigma$ used in the experiment, the corresponding value is $k_\sigma = 1.3$ rad/$\mu$m, and the experimentally found largest value 3.5 rad/$\mu$m corresponds approximately to $3k_\sigma$. The value also confirms that the observed MSSWs are not driven by propagating surface acoustic waves (SAWs) in the GaAs substrate. Indeed, the SAW velocity in a GaAs(001) substrate is 2.7 km/s [51], which gives a maximum SAW frequency of 1.5 GHz at a wave number of 3.5 rad/$\mu$m. The value is well below the frequencies of the excited MSSWs.

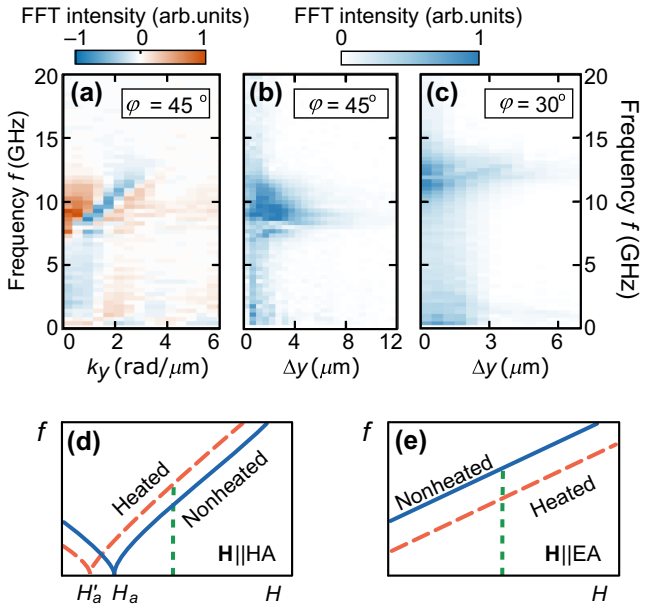


FIG. 4. (a) Dispersion of MSSWs reconstructed via 2D FFT (real part) at $\varphi = 45°$. (b),(c) FFT spectra at different pump-probe shifts $\Delta y$ at $\varphi = 45°$ and 30°. (d),(e) Schematic representation of the frequency changes in the heated area when **H** is along a hard (HA) and easy (EA) anisotropy axis, respectively. Solid lines denote dependences of $f(H)$ for a nonheated film and dashed lines $f'(H)$ for a heated film. Vertical dashed lines represent the magnitude of **H** in the experiments.

It is important to note that the laser-induced heating and the changes of magnetization and anisotropy are expected to alter the precession frequency $f$ within the pump spot. These changes, indeed, can be clearly seen in $f - \Delta y$ maps, where $f$ is obtained as the FFT of $\theta_K(t)$ at a specific position $\Delta y$ [Figs. 4(b) and 4(c)]. For **H** applied along the hard axis ($\varphi = 45°$), $f$ experiences an increase inside the heated area. If **H** is not aligned with the hard axis (e.g., at $\varphi = 30°$), the situation is opposite, and $f$ is decreased inside the pump spot. Both observations are in agreement with the scenario of the magnetic anisotropy being decreased abruptly within the laser-excited spot. Indeed, in the hard-hard configuration, the laser-induced ultrafast heating partly suppresses the effective anisotropy field $H_a$, resulting in an increase of $f$ at $H > H_a$, as schematically illustrated in Fig. 4(d). The opposite situation is expected in the "easy-easy" configuration [see Fig. 4(e)].

It should be noted that the laser-induced local decrease of the eigenfrequency $f_0$ can lead to the formation of a

potential well for MSSWs, with eigenfrequencies below the spectrum of MSSWs outside this well, as demonstrated in Ref. [52]. Then the escape of the MSSWs from this well would be strongly suppressed. We do not observe the formation of such traps as they are formed when the diameter of the hot spot is several times larger than the MSSW wavelength. In our pump-probe experiments, the shortest excited MSSW wavelength is comparable to the pump spot size. In other words, when the pump spot size becomes comparable to the length scale defined by the ratio of the group velocity of a MSSW to $f_0$, the precession of the magnetization propagates as MSSWs from the pump spot to the nonexcited area [27].

### E. Theoretical analysis

#### *1. Dispersion of magnetostatic waves in an anisotropic film*

In order to obtain the expression for the spin wave dispersion $f(\mathbf{k})$, we utilize the approach developed in Ref. [53] and adapt it to the particular anisotropy of the studied film. The basic expression for the film's free-energy density used in our calculations has the form

$$\Delta F = K_1(m_1^2m_2^2 + m_1^2m_3^2 + m_2^2m_3^2) + K_u m_1 m_2 - \mu_0 M_s \hat{\mathbf{m}} \cdot \mathbf{H}, \tag{4}$$

where $\hat{\mathbf{m}}$ is the unit vector in the magnetization direction, and $m_i$ is its projection on the crystallographic axis $x_i$ (see inset in Fig. 1). The form of the in-plane anisotropy term $K_u m_1 m_2$ is chosen after Ref. [38] to accommodate our system of an iron-based alloy grown on a GaAs(001) substrate. Note that Eq. (4) does not contain the magnetostatic energy term. In the derivation of the dispersion relation, the demagnetizing field is accounted for separately by solving the Maxwell equations. Applying the procedures described in Ref. [53] to the free-energy density given by Eq. (4), we obtain a transcendental equation connecting $f$ and $\mathbf{k}$, which can be simplified and written in a closed form in the limit $kd \ll 1$ relevant in our case [54], yielding the dispersion relation for magnetostatic waves to be

$$\omega(\mathbf{k}) = 2\pi f(\mathbf{k}) \approx \gamma \sqrt{\left[B_\alpha + \mu_0 M_s\left(1 - \frac{kd}{2}\right)\right]\left(B_\beta + \mu_0 M_s \frac{kd}{2}\sin^2\psi\right)}, \tag{5}$$

with $B_\alpha$ and $B_\beta$ defined as

$$B_\alpha = \mu_0 H\cos(\varphi - \varphi_m) - \frac{K_u}{M_s}\sin(2\varphi_m) + \frac{2K_1}{M_s}\left[1 - \frac{1}{2}\sin^2(2\varphi_m)\right],$$
$$B_\beta = \mu_0 H\cos(\varphi - \varphi_m) - \frac{2K_u}{M_s}\sin(2\varphi_m) + \frac{2K_1}{M_s}\cos(4\varphi_m), \tag{6}$$

where $\psi$ is the angle between the equilibrium magnetization and $\mathbf{k}$ (see inset in Fig. 1), $\gamma = 1.76 \times 10^{11}$ rad s$^{-1}$ T$^{-1}$ is the electron's gyromagnetic ratio, and $\varphi_m$ is the angle between the magnetization and the [100] axis obtained from the equilibrium condition

$$\mu_0 H\sin(\varphi - \varphi_m) - \frac{K_1}{2M_s}\sin(4\varphi_m) - \frac{K_u}{M_s}\cos(2\varphi_m) = 0. \tag{7}$$

The discrepancy between the solution of the exact transcendental equation for $f(\mathbf{k})$ and its approximation (5) is negligible at $k < 5$ rad/$\mu$m and $d = 20$ nm. We note that at $k = 0$, i.e., in the case of a homogeneous magnetization precession, Eq. (5) gives exactly the same dependence $f_0(\varphi)$ as the analytical formula for ferromagnetic resonance frequency in a thin anisotropic film [55].

Having obtained the explicit dispersion relation, we derive the expression for the precession ellipticity:

$$\epsilon = \frac{|\Delta M_{xy}|}{|\Delta M_z|} = \sqrt{\frac{|B_\alpha + \mu_0 M_s(1 - kd/2)|}{|B_\beta + \mu_0 M_s(kd/2)\sin^2\psi|}}, \tag{8}$$

where $\Delta M_{xy}$ and $\Delta M_z$ are the changes of in-plane and out-of-plane magnetization components caused by the precession, respectively. The damping factor as a function of $\varphi$ and $\mathbf{k}$ can be found using the relation [56]

$$\alpha = \alpha_0 \frac{\partial\omega(\mathbf{k})}{\partial\omega_H}, \tag{9}$$

where $\alpha_0$ is the Gilbert damping of the Larmor precession with the frequency $\omega_H = \gamma\mu_0 H$ in the external field $\mathbf{H}$ at $k = 0$ without accounting for demagnetization effects and anisotropy. It is interesting to note that Eq. (9) leads to an anisotropic damping with higher and lower values when

the magnetization is aligned along the hard and easy axes, respectively.

Once the Gilbert damping parameter is known, the formula for the propagation length $L_{\text{prop}}$ can be written in a straightforward way as

$$L_{\text{prop}} = \tau v_{\text{gr}} = \frac{1}{\alpha\omega(\mathbf{k})}\frac{\partial\omega(\mathbf{k})}{\partial\mathbf{k}}, \tag{10}$$

where $\tau$ is the relaxation time and $v_{\text{gr}}$ is the group velocity of the MSSW.

#### *2. Analysis of the magnetization precession within the excitation spot*

In order to apply the expressions derived above for a description of the experimentally observed magnetization dynamics, one needs to account for the timescales of the laser-induced changes of magnetic anisotropy and magnetization. In metals, a few picoseconds after excitation, both magnetization and magnetic anisotropy possess slow relaxations that can be neglected on the timescales where the precession is observed. Thus, the temporal profile of the effective magnetocrystalline anisotropy field governed by the factors $K_1/M_s$ and $K_u/M_s$ is described below by the Heaviside function.

By analyzing the experimental dependences $f_0(\varphi)$ and $A^0_{\text{SW}}(\varphi)$ within the pump spot, we extract the anisotropy parameters $K_1$ and $K_u$ and saturation magnetization $M_s$ of the excited and equilibrium film using the following procedure. First, the frequency $f_0$ within the pump spot is defined by modified parameters $K_1$, $K_u$, and $M_s$ of the laser-exited material. Fitting the experimental dependence $f_0(\varphi)$ by Eq. (5) with $k = 0$ [solid line in Fig. 3(a)], we get $\mu_0 M_s = 1.56$ T, $K_1 = 2.8 \times 10^4$ J/m$^3$, and $K_u = -1 \times 10^4$ J/m$^3$.

Having determined the parameters of the film within the laser-excited area, we now can extract the laser-induced changes of the anisotropy parameters $K_1$ and $K_u$ with respect to their room temperature (RT) values by analyzing the azimuthal dependence $A^0_{\text{SW}}(\varphi)$ of the laser-excited precession [Fig. 3(b)]. Indeed, two sets of the parameters, the initial $\tilde{K}_1$, $\tilde{K}_u$, and $\tilde{M}_s$ at RT and the modified $K_1$, $K_u$, and $M_s$ of the laser-excited film, yield the difference between the effective field orientations at equilibrium and upon the excitation. This difference defines the amplitude of the in-plane component $\Delta M^0_{xy}$ of the precession. The amplitude of the out-of-plane component $\Delta M^0_z$ can then be found by taking into account the precession ellipticity defined by Eq. (8). The fitting of $A^0_{\text{SW}}(\varphi) \sim \Delta M^0_z$ then gives the ratios $\tilde{K}_1/\tilde{M}_s$ and $\tilde{K}_u/\tilde{M}_s$. Using the experimental value of the RT saturation magnetization $\mu_0\tilde{M}_s = 1.7$ T [57,58], we obtain the RT anisotropy parameters $\tilde{K}_1 = 3.33 \times 10^4$ J/m$^3$ and $\tilde{K}_u = -1.03 \times 10^4$ J/m$^3$, which are in a very good agreement with the anisotropy parameters found earlier for a 22-nm $Fe_{0.81}Ga_{0.19}$ film on a GaAs(001) substrate [58]. We note that the laser-induced change $\Delta K_1/\tilde{K}_1 \approx -16\%$ shows rather good agreement with the one reported earlier for a 100-nm Galfenol film [41], while $\Delta M_s/\tilde{M}_s \approx -8\%$ agrees with the magnitude of the ultrafast demagnetization observed in a thinner Galfenol film [42].

#### *3. Analysis of the laser-driven spin wave propagation*

In order to explain the observed azimuthal dependence $L_{\text{prop}}(\varphi)$, we use Eq. (10). The fitting procedure at $k = 1$ rad/$\mu$m gives the Gilbert damping parameter $\alpha_0 = 0.017$. As can be seen in Fig. 3(d), Eqs. (9) and (10) correctly predict the azimuthal dependence of the MSSW propagation. In particular, the theory confirms that the different propagation lengths for different angles between **H** and the MSSW wave vector are dictated by the anisotropy of the film. We note that the observed anisotropy of the propagation of the laser-driven MSSW packets is in agreement with the one demonstrated in cubic iron films recently [59]. In both cases, the largest propagation length is observed in the hard-hard configuration. In contrast to the experiments with antennae [59], where the MSSW propagation is one dimensional, laser-induced MSSW packets propagating along the $y$ axis are spreading slightly along the $x$ axis as well. Our results show that this spreading does not change the main features of the propagation of MSSW packets.

Theoretically obtained MSSW group velocities $v_{\text{gr}}$ are in the range of 5–9 km/s, which is in agreement with the experimental values of 4.5–13 km/s. These values of group velocities are typical for MSSWs in thin metallic films [3].

Finally, having obtained the MSSW parameters, including the anisotropic damping $\alpha$, we calculate spatial-temporal $\Delta y$-$t$ maps at different $\varphi$ following the procedure described in Refs. [18,21,24,27]. In this approach, the dispersion relation (5) for MSSWs is used. Within the area corresponding to the excitation spot, the additional effective field with the Heaviside temporal and Gaussian spatial profiles is introduced to account for the localized change of magnetic anisotropy triggering the precession (see the Appendix for details). Figure 2(f) shows exemplary cross sections of the calculated $\Delta y$-$t$ maps demonstrating good agreement with the experimental data. The calculations show good agreement with the experimentally obtained precession and MSSW packets [Figs. 2(c) and 2(f)]. Importantly, the calculations reveal the same deviation of the MSSW packet shapes from the Gaussian ones as the experimentally observed signals $\Delta\theta_K(t)$, evident in Figs. 2(c) and 2(f). The most prominent deviation is observed at large time delays $t$, i.e., at the tails of the wave packets, as noted by other groups as well [26,27,60]. Our calculations based on the MSSW dispersion relation show that this deviation originates from the dispersion of SWs generated by a sudden change of effective field.

## IV. CONCLUSION

In conclusion, we demonstrate laser-induced excitation and propagation of magnetostatic spin waves in a 20-nm-thick epitaxial Galfenol film on a GaAs substrate characterized by pronounced in-plane magnetic anisotropy. We show that ultrafast thermal magnetic anisotropy changes induced by tightly focused femtosecond laser pulses excite propagating MSSWs. The strong in-plane anisotropy (order of magnitude of $10^4$ J/m$^3$) of the film enables the laser-induced excitation of MSSWs in a simple geometry with an in-plane external magnetic field. The anisotropy of the film provides the possibility to tune the frequency, amplitude, and propagation length of the excited waves by changing the in-plane field orientation. We find that the propagation length of the MSSWs in the studied film reaches 3.4 $\mu$m, which, along with other recent results on spin dynamics in Galfenol films [40,42,61], confidently promotes epitaxial Galfenol to the limited family of metallic materials for magnonics. Furthermore, epitaxial Galfenol is also known for having a large magnetoelastic constant and saturation magnetostriction [58] and so offers the prospect of controlling the SW propagation via a voltage-induced strain when, for example, coupled to a piezoelectric substrate, as realized earlier in yttrium iron garnet [11]. It is important to note that the laser-induced thermal magnetocrystalline anisotropy change can be applied to a broad range of materials without limitations on their electronic and magnetic structures. Finally, we note that introducing laser-induced ultrafast thermal changes of magnetic anisotropy as a tool to generate SWs can have an even broader impact on magnonics. Since abrupt and local changes of the magnetic anisotropy by laser pulses yield strong local modifications of the SW dispersion relation, they can be seen as a pathway to realize an ultrafast optically reconfigurable magnonic medium for efficient steering and conversion of SWs [15,16,62,63].

## ACKNOWLEDGMENTS

The authors thank L.V. Lutsev and I.V. Savochkin for valuable discussions. The setup construction and experiments are carried out by N.E.Kh., L.A.S., A.V.S., and A.M.K. under the support of the RSF (Grant No. 16-12-10485); theoretical analysis and calculations are supported in part by the RFBR (Grant No. 18-02-00824 awarded to N.E.Kh., P.I.G., and A.V.A.). Collaboration between the Ioffe Institute and TU Dortmund (N.E.Kh., L.A.S., A.V.S., and A.M.K.) is a part of the TRR 160 ICRC "Coherent manipulation of interacting spin excitations in tailored semiconductors" supported jointly by the RFBR (Grant No. 19-52-12065) and DFG, and of the COST action CA17123 Magnetofon.

## APPENDIX: CALCULATION OF SPATIAL-TEMPORAL MAPS OF LASER-DRIVEN SPIN WAVES

To calculate the spatial-temporal dependences of $\Delta\theta_K(\mathbf{r}, t)$ corresponding to the experimental $\Delta y$-$t$ maps,

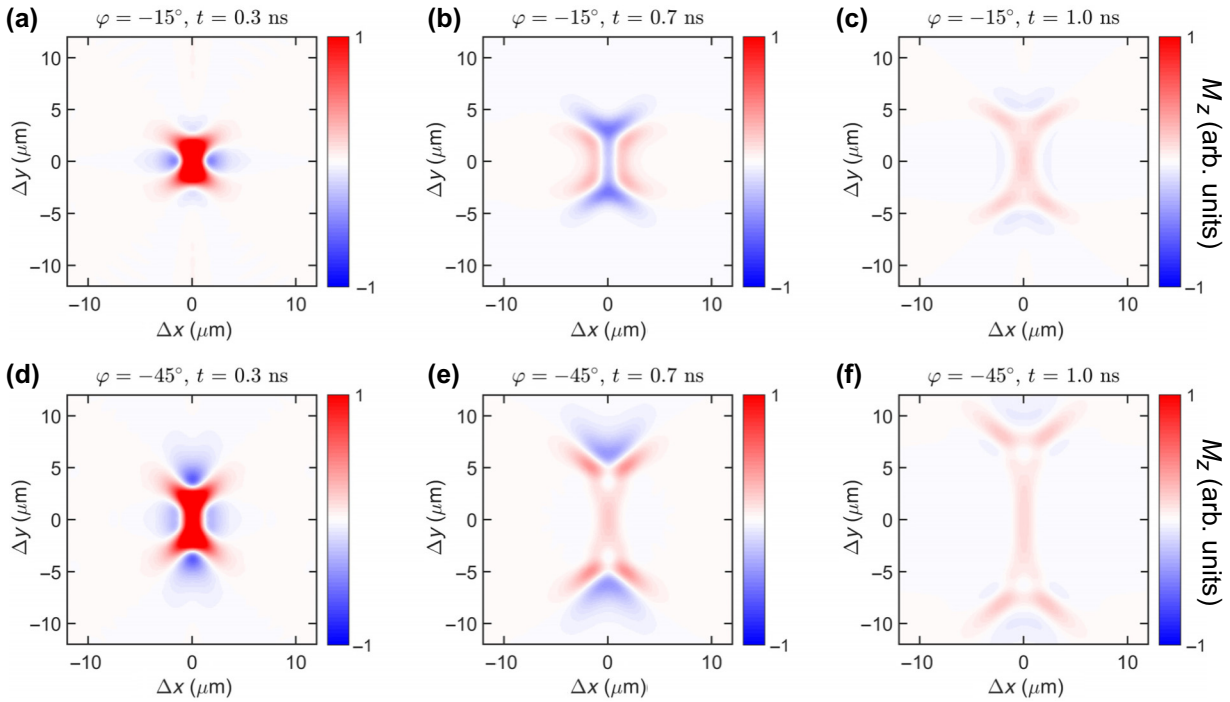


FIG. 5. Calculated SW signals in the $x$-$y$ plane at different time delays $t$ after the excitation, 0.3 ns (a),(d), 0.7 ns (b),(e), and 1 ns (c),(f) for the angles $\varphi$ of $-15°$ (a)–(c) and $-45°$ (d)–(f).

we use the procedure described in Refs. [18,21,24,27]. The probe pulses are reflected normally, so the change of their polarization is a measure of the transient changes of the out-of-plane component $M_z$. The normal component is given by an integration over all excited wave vectors $\mathbf{k} = (k_x, k_y)$ [27]:

$$M_z(\mathbf{r}, t) \sim \int d\mathbf{k}(1/\epsilon)h(\mathbf{k}, \omega)\sin[\mathbf{k}\cdot\mathbf{r} - \omega(\mathbf{k})t] \times \exp[-\alpha\omega(\mathbf{k})t], \quad \text{(A1)}$$

where $h(\mathbf{k}, \omega)$ is the Fourier transform of $h(\mathbf{r}, t)$, an effective field describing the effect of the laser pulse excitation of the sample; $\epsilon$ is the ellipticity (8); and $\alpha$ is the damping parameter (9).

We consider the case of *thermal* changes of anisotropy, which are approximated by the laser-induced effective field introduced as the difference between the total effective field in the equilibrium and laser-excited states $\mu_0 h(\mathbf{r}, t) = -\partial\Delta F(\tilde{K}_1, \tilde{K}_u, \tilde{M}_s)/\partial\mathbf{M} + \partial\Delta F\,(K_1(\mathbf{r}, t), K_u(\mathbf{r}, t), M_s(\mathbf{r}, t))/\partial\mathbf{M}$ [45]. It is assumed that, a few picoseconds after excitation, both the magnetization and magnetic anisotropy possess slow relaxation that can be neglected on the timescales of the magnetization precession. Thus, the field $h(\mathbf{r}, t)$ may be rewritten as $h(\mathbf{r}, t) \sim h(\mathbf{r})\Theta(t)$, where $\Theta(t)$ is a Heaviside function. Hence, the Fourier transform $h(\mathbf{k}, \omega)$ at $\omega \neq 0$ is weighted by $i/\omega$ [24]. Next, the pump beam in our experiments has a spatial profile close to the Gaussian one, i.e., $h(\mathbf{r}) \sim \exp[-\mathbf{r}^2/(2\sigma^2)]$. Therefore, $h(\mathbf{k}, \omega) \sim \exp(-\mathbf{k}^2\sigma^2/2)$. Thus, $k'_\sigma = \sqrt{2}/\sigma$ gives a wave number for the excited SW component whose amplitude is at a level $1/\sqrt{e}$ of the component with the highest amplitude. It is also important to take into account that the probe spot radius in our experiment is $\sigma$ as well. As a result, the measured wave numbers are defined by an effective width of $\sqrt{2}\sigma$ [27], and the corresponding wave number is $k_\sigma = 1/\sigma$.

Using the procedure described above, the maps of $M_z(\mathbf{r}, t)$ are calculated in the time interval 0–1.5 ns for different $\varphi$. Calculations are performed for $k_x$ and $k_y$ with an upper limit of 5.3 rad/$\mu$m, which exceeds the value $3k_\sigma$. Calculated $\Delta y$-$t$ maps are in good agreement with the experiment.

Figure 5 shows the calculated $z$ component of the magnetization as a function of $\Delta x$ and $\Delta y$ at different time delays $t = 0.3$, 0.7, and 1 ns (see also the Supplemental Material [64]). Excited SWs are mainly propagating in the $y$ direction with a pronounced X-shaped pattern. Similar two-dimensional maps for a permalloy film are discussed in the Supplemental Material of Ref. [26]. Slight spreading of the SWs in the $x$ direction is clearly seen.


[1] B. Lenk, H. Ulrichs, F. Garbs, and M. Münzenberg, The building blocks of magnonics, Phys. Rep. **507**, 107 (2011).

[2] S. A. Nikitov, D. V. Kalyabin, I. V. Lisenkov, A. N. Slavin, Y. N. Barabanenkov, S. A. Osokin, A. V. Sadovnikov, E. N. Beginin, M. A. Morozova, Y. P. Sharaevsky, Y. A. Filimonov, Y. V. Khivintsev, S. L. Vysotsky, V. K. Sakharov, and E. S. Pavlov, Magnonics: A new research area in spintronics and spin wave electronics, Phys. Usp. **58**, 1002 (2015).

[3] A. V. Chumak, A. A. Serga, and B. Hillebrands, Magnonic crystals for data processing, J. Phys. D: Appl. Phys. **50**, 244001 (2017).

[4] V. E. Demidov, S. Urazhdin, R. Liu, B. Divinskiy, A. Telegin, and S. O. Demokritov, Excitation of coherent propagating spin waves by pure spin currents, Nat. Commun. **7**, 10446 (2016).

[5] D. Ralph and M. Stiles, Spin transfer torques, J. Magn. Magn. Mater. **320**, 1190 (2008).

[6] F. Hellman *et al.*, Interface-induced phenomena in magnetism, Rev. Mod. Phys. **89**, 025006 (2017).

[7] D. Grundler, Reconfigurable magnonics heats up, Nature Phys. **11**, 438 (2015).

[8] C. S. Davies and V. V. Kruglyak, Graded-index magnonic, Low Temp. Phys. **41**, 760 (2015).

[9] A. V. Chumak, V. I. Vasyuchka, A. A. Serga, and B. Hillebrands, Magnon spintronics, Nat. Phys. **11**, 453 (2015).

[10] S. J. Hämäläinen, M. Madami, H. Qin, G. Gubbiotti, and S. van Dijken, Control of spin-wave transmission by a programmable domain wall, Nat. Commun. **9**, 4853 (2018).

[11] A. V. Sadovnikov, A. A. Grachev, S. E. Sheshukova, Y. P. Sharaevskii, A. A. Serdobintsev, D. M. Mitin, and S. A. Nikitov, Magnon Straintronics: Reconfigurable Spin-wave Routing in Strain-controlled Bilateral Magnetic Stripes, Phys. Rev. Lett. **120**, 257203 (2018).

[12] V. F. Kovalenko and E. L. Nagaev, Photoinduced magnetism, Sov. Phys. Usp. **29**, 297 (1986).

[13] A. Kirilyuk, A. V. Kimel, and T. Rasing, Ultrafast optical manipulation of magnetic order, Rev. Mod. Phys. **82**, 2731 (2010).

[14] B. Lenk, F. Garbs, H. Ulrichs, N. Abeling, and M. Münzenberg, in *Magnonics. Topics in Applied Physics*, edited by S. O. Demokritov and A. Slavin (Springer, Berlin, Heidelberg, 2013), Vol. 125, Chap. 10, p. 71.

[15] M. Vogel, A. V. Chumak, E. H. Waller, T. Langner, V. I. Vasyuchka, B. Hillebrands, and G. von Freymann, Optically-reconfigurable magnetic materials, Nat. Phys. **11**, 487 (2015).

[16] M. Vogel, R. Aßmann, P. Pirro, A. V. Chumak, B. Hillebrands, and G. von Freymann, Control of spin-wave propagation using magnetisation gradients, Sci. Rep. **8**, 11099 (2018).

[17] Y. Au, M. Dvornik, T. Davison, E. Ahmad, P. S. Keatley, A. Vansteenkiste, B. Van Waeyenberge, and V. V. Kruglyak, Direct Excitation of Propagating Spin Waves by Focused Ultrashort Optical Pulses, Phys. Rev. Lett. **110**, 097201 (2013).

[18] T. Satoh, Y. Terui, R. Moriya, B. A. Ivanov, K. Ando, E. Saitoh, T. Shimura, and K. Kuroda, Directional control of

spin-wave emission by spatially shaped light, Nat. Photonics **6**, 662 (2012).

[19] D. Bossini, S. Dal Conte, Y. Hashimoto, A. Secchi, R. V. Pisarev, T. Rasing, G. Cerullo, and A. V. Kimel, Macrospin dynamics in antiferromagnets triggered by sub-20 femtosecond injection of nanomagnons, Nature Comm. **7**, 10645 (2016).

[20] C. L. Chang, S. Mieszczak, M. Zelent, V. Besse, U. Martens, R. R. Tamming, J. Janusonis, P. Graczyk, M. Münzenberg, J. W. Kłos, and R. I. Tobey, Driving Magnetization Dynamics in an On-demand Magnonic Crystal via the Magnetoelastic Interactions, Phys. Rev. Appl. **10**, 064051 (2018).

[21] I. V. Savochkin, M. Jäckl, V. I. Belotelov, I. A. Akimov, M. A. Kozhaev, D. A. Sylgacheva, A. I. Chernov, A. N. Shaposhnikov, A. R. Prokopov, V. N. Berzhansky, D. R. Yakovlev, A. K. Zvezdin, and M. Bayer, Generation of spin waves by a train of fs-laser pulses: A novel approach for tuning magnon wavelength, Sci. Rep. **7**, 5668 (2017).

[22] M. Jäckl, V. I. Belotelov, I. A. Akimov, I. V. Savochkin, D. R. Yakovlev, A. K. Zvezdin, and M. Bayer, Magnon Accumulation by Clocked Laser Excitation as Source of Long-range Spin Waves in Transparent Magnetic Films, Phys. Rev. X **7**, 021009 (2017).

[23] A. I. Chernov, M. A. Kozhaev, I. V. Savochkin, D. V. Dodonov, P. M. Vetoshko, A. K. Zvezdin, and V. I. Belotelov, Optical excitation of spin waves in epitaxial iron garnet films: MSSW vs BVMSW, Opt. Lett. **42**, 279 (2017).

[24] Y. Hashimoto, S. Daimon, R. Iguchi, Y. Oikawa, K. Shen, K. Sato, D. Bossini, Y. Tabuchi, T. Satoh, B. Hillebrands, G. E. W. Bauer, T. H. Johansen, A. Kirilyuk, T. Rasing, and E. Saitoh, All-optical observation and reconstruction of spin wave dispersion, Nat. Commun. **8**, 15859 (2017).

[25] I. Yoshimine, T. Satoh, R. Iida, A. Stupakiewicz, A. Maziewski, and T. Shimura, Phase-controllable spin wave generation in iron garnet by linearly polarized light pulses, J. Appl. Phys. **116**, 043907 (2014).

[26] S. Iihama, Y. Sasaki, A. Sugihara, A. Kamimaki, Y. Ando, and S. Mizukami, Quantification of a propagating spin-wave packet created by an ultrashort laser pulse in a thin film of a magnetic metal, Phys. Rev. B **94**, 020401(R) (2016).

[27] A. Kamimaki, S. Iihama, Y. Sasaki, Y. Ando, and S. Mizukami, Reciprocal excitation of propagating spin waves by a laser pulse and their reciprocal mapping in magnetic metal films, Phys. Rev. B **96**, 014438 (2017).

[28] S.-J. Yun, C.-G. Cho, and S.-B. Choe, Simultaneous excitation of two different spinwave modes by optical ultrafast demagnetization, Appl. Phys Express **8**, 063009 (2015).

[29] Z. Chen, Y. Yan, S. Li, X. Xu, Y. Jiang, and T. Lai, Simultaneous laser excitation of backward volume and perpendicular standing spin waves in full-Heusler $Co_2FeAl_{0.5}Si_{0.5}$ films, Sci. Rep. **7**, 42513 (2017).

[30] Y. Hashimoto, D. Bossini, T. H. Johansen, E. Saitoh, A. Kirilyuk, and T. Rasing, Frequency and wavenumber selective excitation of spin waves through coherent energy transfer from elastic waves, Phys. Rev. B **97**, 140404(R) (2018).

[31] N. Ogawa, W. Koshibae, A. J. Beekman, N. Nagaosa, M. Kubota, M. Kawasaki, and Y. Tokura, Photodrive of magnetic bubbles via magnetoelastic waves, Proc. Natl. Acad. Sci. U.S.A. **112**, 8977 (2015).

[32] Y. Hashimoto, T. H. Johansen, and E. Saitoh, 180°-phase shift of magnetoelastic waves observed by phase-resolved spin-wave tomography, Appl. Phys. Lett. **112**, 232403 (2018).

[33] T. Hioki, Y. Hashimoto, T. H. Johansen, and E. Saitoh, Time-resolved Imaging of Magnetoelastic Waves by the Cotton-Mouton Effect, Phys. Rev. Appl. **11**, 061007 (2019).

[34] P. G. Baranov, A. M. Kalashnikova, V. I. Kozub, V. L. Korenev, Y. G. Kusrayev, R. V. Pisarev, V. F. Sapega, I. A. Akimov, M. Bayer, A. V. Scherbakov, and D. R. Yakovlev, Spintronics of semiconductor, metallic, dielectric, and hybrid structures, Phys. Usp. **62** (2019).

[35] T. L. Linnik, V. N. Kats, J. Jäger, A. S. Salasyuk, D. R. Yakovlev, A. W. Rushforth, A. V. Akimov, A. M. Kalashnikova, M. Bayer, and A. V. Scherbakov, The effect of dynamical compressive and shear strain on magnetic anisotropy in a low symmetry ferromagnetic film, Phys. Scr. **92**, 054006 (2017).

[36] J. J. Krebs, B. T. Jonker, and G. A. Prinz, Properties of Fe single-crystal films grown on (100)GaAs by molecular-beam epitaxy, J. Appl. Phys. **61**, 2596 (1987).

[37] M. Gester, C. Daboo, R. J. Hicken, S. J. Gray, A. Ercole, and J. A. C. Bland, Continuous evolution of the in-plane magnetic anisotropies with thickness in epitaxial Fe films, J. Appl. Phys. **80**, 347 (1996).

[38] G. Wastlbauer and J. A. C. Bland, Structural and magnetic properties of ultrathin epitaxial Fe films on GaAs(001) and related semiconductor substrates, Adv. Phys. **54**, 137 (2005).

[39] A. T. Hindmarch, Interface magnetism in ferromagnetic metal-compound semiconductor hybrid stractures, SPIN **1**, 45 (2011).

[40] A. P. Danilov, A. V. Scherbakov, B. A. Glavin, T. L. Linnik, A. M. Kalashnikova, L. A. Shelukhin, D. P. Pattnaik, A. W. Rushforth, C. J. Love, S. A. Cavill, D. R. Yakovlev, and M. Bayer, Optically excited spin pumping mediating collective magnetization dynamics in a spin valve structure, Phys. Rev. B **98**, 060406(R) (2018).

[41] V. N. Kats, T. L. Linnik, A. S. Salasyuk, A. W. Rushforth, M. Wang, P. Wadley, A. V. Akimov, S. A. Cavill, V. Holy, A. M. Kalashnikova, and A. V. Scherbakov, Ultrafast changes of magnetic anisotropy driven by laser-generated coherent and noncoherent phonons in metallic films, Phys. Rev. B **93**, 214422 (2016).

[42] A. V. Scherbakov, A. P. Danilov, F. Godejohann, T. L. Linnik, B. A. Glavin, L. A. Shelukhin, D. P. Pattnaik, M. Wang, A. W. Rushforth, D. R. Yakovlev, A. V. Akimov, and M. Bayer, Optical Excitation of Single- and Multimode Magnetization Precession in Fe–Ga Nanolayers, Phys. Rev. Appl. **11**, 031003 (2019).

[43] E. Carpene, E. Mancini, D. Dazzi, C. Dallera, E. Puppin, and S. De Silvestri, Ultrafast three-dimensional magnetization precession and magnetic anisotropy of a photoexcited thin film of iron, Phys. Rev. B **81**, 060415(R) (2010).

[44] T. P. Ma, S. F. Zhang, Y. Yang, Z. H. Chen, H. B. Zhao, and Y. Z. Wu, Distinguishing the laser-induced spin precession excitation mechanism in Fe/MgO(001) through field orientation dependent measurements, J. Appl. Phys. **117**, 013903 (2015).

[45] L. A. Shelukhin, V. V. Pavlov, P. A. Usachev, P. Y. Shamray, R. V. Pisarev, and A. M. Kalashnikova, Ultrafast laser-induced changes of the magnetic anisotropy in a low-symmetry iron garnet film, Phys. Rev. B **97**, 014422 (2018).

[46] E. Beaurepaire, J.-C. Merle, A. Daunois, and J.-Y. Bigot, Ultrafast Spin Dynamics in Ferromagnetic Nickel, Phys. Rev. Lett. **76**, 4250 (1996).

[47] C. Zener, Classical theory of the temperature dependence of magnetic anisotropy energy, Phys. Rev. **96**, 1335 (1954).

[48] M. van Kampen, C. Jozsa, J. T. Kohlhepp, P. LeClair, L. Lagae, W. J. M. de Jonge, and B. Koopmans, All-optical Probe of Coherent Spin Waves, Phys. Rev. Lett. **88**, 227201 (2002).

[49] A. M. Kalashnikova, A. V. Kimel, and R. V. Pisarev, Ultrafast opto-magnetism, Phys. Usp. **58**, 969 (2015).

[50] A. V. Azovtsev and N. A. Pertsev, Magnetization dynamics and spin pumping induced by standing elastic waves, Phys. Rev. B **94**, 184401 (2016).

[51] A. A. Maznev, A. M. Lomonosov, P. Hess, and A. A. Kolomenskii, Anisotropic effects in surface acoustic wave propagation from a point source in a crystal, Eur. Phys. J. B **35**, 429 (2003).

[52] O. Kolokoltsev, N. Qureshi, E. Mejía-Uriarte, and C. L. Ordóñez-Romero, Hot spin-wave resonators and scatterers, J. Appl. Phys. **112**, 013902 (2012).

[53] M. Hurben and C. Patton, Theory of magnetostatic waves for in-plane magnetized anisotropic films, J. Magn. Magn. Mater. **163**, 39 (1996).

[54] L. R. Walker, Magnetostatic modes in ferromagnetic resonance, Phys. Rev. **105**, 390 (1957).

[55] A. V. Azovtsev and N. A. Pertsev, Electrical Tuning of Ferromagnetic Resonance in Thin-film Nanomagnets Coupled to Piezoelectrically Active Substrates, Phys. Rev. Appl. **10**, 044041 (2018).

[56] D. D. Stancil and A. Prabhakar, *Spin Waves: Theory and Applications* (Springer, New York, 2009).

[57] D. B. Gopman, V. Sampath, H. Ahmad, S. Bandyopadhyay, and J. Atulasimha, Static and dynamic magnetic properties of sputtered Fe–Ga thin films, IEEE Trans. Magn. **53**, 1 (2017).

[58] D. E. Parkes, L. R. Shelford, P. Wadley, V. Holý, M. Wang, A. T. Hindmarch, G. van der Laan, R. P. Campion, K. W. Edmonds, S. A. Cavill, and A. W. Rushforth, Magnetostrictive thin films for microwave spintronics, Sci. Rep. **3**, 2220 (2013).

[59] K. Sekiguchi, S.-W. Lee, H. Sukegawa, N. Sato, S.-H. Oh, R. D. McMichael, and K.-J. Lee, Spin-wave propagation in cubic anisotropy materials, NPG Asia Mater. **9**, e392 (2017).

[60] M. Wu, B. A. Kalinikos, P. Krivosik, and C. E. Patton, Fast pulse-excited spin waves in yttrium iron garnet thin films, J. Appl. Phys. **99**, 013901 (2006).

[61] A. S. Salasyuk, A. V. Rudkovskaya, A. P. Danilov, B. A. Glavin, S. M. Kukhtaruk, M. Wang, A. W. Rushforth, P. A. Nekludova, S. V. Sokolov, A. A. Elistratov, D. R. Yakovlev, M. Bayer, A. V. Akimov, and A. V. Scherbakov, Generation of a localized microwave magnetic field by coherent phonons in a ferromagnetic nanograting, Phys. Rev. B **97**, 060404(R) (2018).

[62] J. Stigloher, M. Decker, H. S. Körner, K. Tanabe, T. Moriyama, T. Taniguchi, H. Hata, M. Madami, G. Gubbiotti, K. Kobayashi, T. Ono, and C. H. Back, Snell's Law for Spin Waves, Phys. Rev. Lett. **117**, 037204 (2016).

[63] A. V. Sadovnikov, E. N. Beginin, S. E. Sheshukova, Y. P. Sharaevskii, A. I. Stognij, N. N. Novitski, V. K. Sakharov, Y. V. Khivintsev, and S. A. Nikitov, Route toward semiconductor magnonics: Light-induced spin-wave nonreciprocity in a YIG/GaAs structure, Phys. Rev. B **99**, 054424 (2019).

[64] See Supplemental Material at http://link.aps.org/supplemental/10.1103/PhysRevApplied.12.044044 with a calculated 2D map of the $z$ component of the magnetization in a movie format.